A pair of esterases from a commensal gut bacterium remove acetylations from all positions on complex β-mannans.

Authors:

Leszek Michalak[1], Sabina Leanti La Rosa[1], Shaun Allan Leivers[1], Lars Jordhøy Lindstad[1],

Åsmund Røhr Kjendseth[1], Finn Lillelund Aachmann[2], Bjørge Westereng[1*]

[1] Faculty of Chemistry, Biotechnology and Food Science, Norwegian University of Life

Sciences, 1432 Ås, Norway

[2] NOBIPOL, Department of Biotechnology and Food Science, NTNU Norwegian University of

Science and Technology, Sem Sælands vei 6-8, N-7491 Trondheim, Norway

* Corresponding author, Bjørge Westereng, bjorge.westereng@nmbu.no

Abstract:

β-Mannans and xylans are important components of the plant cell wall and they are acetylated to be protected from degradation by glycoside hydrolases. β-Mannans are widely present in human and animal diets as fiber from leguminous plants and as thickeners and stabilizers in processed foods. There are many fully characterized acetylxylan esterases (AcXEs), however, the enzymes deacetylating mannans are less understood. Here we present two carbohydrate esterases, *Ri*CE2 and *Ri*CEX, from the Firmicute *Roseburia intestinalis,* which together deacetylate complex galactoglucomannan (GGM)*.* The 3D-structure of *Ri*CEX with a mannopentaose in the active site shows that the CBM35 domain of *Ri*CEX forms a confined complex, where the axially oriented C2-hydroxyl of a mannose residue points towards the Ser41 of the catalytic triad. Cavities on the *Ri*CEX surface may accept galactosylations at the C6 positions of mannose adjacent to the mannose residue being deacetylated (subsite -1 and +1). In depth characterization of the two enzymes using time-resolved NMR, HPLC and mass spectrometry demonstrates that they work in a

31   complementary manner. *Ri*CEX exclusively removes the axially oriented 2-*O*-acetylations on

32   any mannose residue in an oligosaccharide, including double acetylated mannoses, while

33   the *Ri*CE2 is active on 3-*O*-, 4-*O*- and 6-*O*-acetylations. Activity of *Ri*CE2 is dependent on

34   *Ri*CEX removing 2-*O*-acetylations from double acetylated mannose. Furthermore,

35   transacetylation of oligosaccharides with the 2-*O* specific *Ri*CEX provided new insight to how

36   temperature and pH affects acetyl migration on mannooligosaccharides.

37

38   **Significance statement:**

39   Acetylations are an important feature of hemicellulose, altering the physical properties of

40   the plant cell wall, and limiting enzyme accessibility. Removal of acetyl groups from beta-

41   mannan is a key step towards efficient utilization of mannans as a carbon source for gut

42   microbiota and in biorefineries. We present detailed insight into mannan deacetylation by

43   two highly substrate-specific acetyl-mannan esterases (AcMEs) from a prevalent gut

44   commensal Firmicute, which cooperatively deacetylate complex galactoglucomannan. The

45   3D structure of *Ri*CEX with mannopentaose in the active site has a unique two-domain

46   architecture including a CBM35 and an SGNH superfamily hydrolytic domain. Discovery of

47   mannan specific esterases improves the understanding of an important step in dietary fiber

48   utilization by gut commensal Firmicutes.

49

50

51   **Introduction:**

52   Enzymatic acetylation and deacetylation are involved in numerous processes in Nature.

53   N-acetylation of lysine in histones is crucial for the control of gene transcription (1);

54   acetylation or deacetylation of N-acetylglucosamine and N-acetylmuramic acid in microbial

55   peptidoglycan affects its degradation by lysozyme (2). The efficacy of penicillins is also

56   linked to acetylations, e.g. penicillin resistance caused by bacteria expressing cephalosporin

57   esterases (3). Acetylations are important constituents in some of the most abundant

58   polymers on earth like chitin, pectin, xylan and β-mannan (4, 5). Enzymes that process these

59   polymers have adapted to a wide array of structurally diverse targets. Studying the

60   structure-function relationships of acetyl esterases and transferases involved is shedding

61   light on this important and very common covalent modification.

62   β-Mannans are polysaccharides present in the secondary cell walls of plants with a

63   backbone consisting of *β*-1,4-linked D-Man*p* units (Fig. 1). The backbone can be interspersed

64   with *β*-1,4 linked D-Glc*p*, as in konjac glucomannan (*Amorphophallus konjac*), decorated

65   with *α*-1,6-D-Gal*p* as in carob galactomannan (*Ceratonia siliqua*), or contain both glucose

66   and galactose such as the GGM in *Aloe vera* and Norway spruce (*Picea abies*) (6-8).

67   Furthermore, mannans may contain substantial amounts of 2-*O*-, 3-*O*-, and 6-*O*-acetylations

68   on any mannose residue in the chain, as well as 4-*O*-acetylations (rare) on the non-reducing
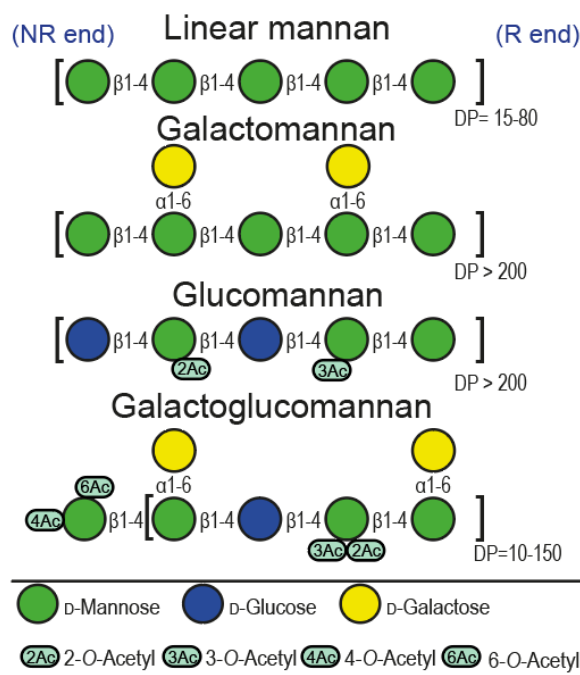
69   end of the chain.

70

71 Fig. 1. A cartoon presentation of various types of mannan found in plants (figure is an adaptation from Fig. 1 in
72 20). Glucomannans like konjac glucomannan generally contain a low degree of acetylation (DA =0.07).
73 Galactoglucomannans contains various DA's, the spruce mannan used in this study (DA = 0.35) and Aloe vera
74 mannan (DA > 0.5).

75

76   Depending on the plant origin, mannans differ in their monosaccharide composition, degree

77   and location of acetylations (9). A unique characteristic of the 2-*O*-acetyl groups of mannans

78   is their relative orientation: 2-*O*-acetylations are axial, as opposed to other common

79   structural polysaccharides, like xylan, pectin and chitin, that all have acetylations in the

80   equatorial plane of the sugar ring.

81   Acetylation of hemicelluloses affects their biological functions and a range of

82   physicochemical properties and is thought to be a defense mechanism developed as a part

83   of an evolutionary arms race against pathogens (5) as well as contributing to aggregation of

84   cellulose microfibrils (10). Acetylations affect the solubility of the polysaccharides by

85   restricting the formation of hydrogen bonds between chains in solution. Effects of mannan

86   acetylations on the viscosity of solutions make them effective thickeners and stabilizers (9,

87   11) in the food and feed industry where mannans such as guar gum and konjac are

88   commonly used (12, 13). Furthermore, the immunostimulatory properties of *Aloe vera* (AV)

89   mannan, a common ingredient in nutraceuticals and cosmetics, have been linked to its high

90   degree of acetylation (8). In the context of biorefining, acetylations reduce fermentability

91   (14) and enzymatic degradability, and thus pose a limitation on the utilization of mannans as

92   a feedstock for fermentation. In this respect, deacetylation of mannan by chemical

93   pretreatment or enzymatic treatment with acetyl esterases is known to improve

94   fermentation yields. On the other hand, the recalcitrance resulting from the presence of

95   acetylations also restricts the number of gut microbes able to consume hemicellulose. This

96   may be beneficial as means of providing selective growth of bacteria when hemicellulose is

97   considered as an ingredient of food and feed.

98   Gut microbes are highly adapted to fermenting diet-derived complex carbohydrates

99   and have evolved complex machineries called polysaccharide utilization loci (PULs) to utilize

100   these carbohydrates (15, 16). Bacteroidetes and Firmicutes are the main polysaccharide

101   degrading commensal bacteria in the human gut (17, 18). β-mannans constitute a small but

102   significant part of human diet that can be found in a wide range of different food products.

103   This may explain why mannan degradation is identified as one of the core pathways in the

104   human gut microbiome (19). Some species of Firmicutes, such as *Roseburia intestinalis*, have

105   developed sophisticated enzymatic machineries for complete β-mannan degradation; these

106   PULs quite frequently contain esterases (20).

107   The esterases deacetylating xylan and mannan characterized so far have been classified

108   together as acetylxylan esterases (EC 3.1.1.72). Carbohydrate esterases (CEs) are common in

109   bacterial and fungal genomes and are often found in PULs together with glycoside

110   hydrolases (GH) (20, 21). This highlights their biological role as accessory enzymes

111   facilitating the processing of glycans. CEs are classified into 16 families according to the

112   CAZy database (22), in which members of families 1-7 and 16 have been reported to be

113   active on hemicelluloses in plant biomass. All CEs, with the exception of family CE4, are

114   serine-histidine hydrolases (5). Esterases from the CE2 family share a two-domain

115   architecture consisting of a catalytic SGNH hydrolase superfamily domain with a conserved

116   catalytic dyad, and an accessory jelly roll domain (23). The two-domain structure results in

117   an open active site able to accommodate a variety of substrates. So far, functionally

118   characterized CE2 esterases have been largely non-specific; activities has been reported on

119   2-*O*-, 3-*O*- and 4-*O*- acetylated xylan, konjac glucomannan (24), and 6-*O*-acetylated mannan

120   (5). Some CE2 esterases have been considered specific to 6-*O*- acetylations, which is the

121   position they transacetylate when using vinyl acetate as the acetate donor (25). Enzymatic

122   deacetylation of mannans has previously been described in literature (26, 27), but no

123   esterase exclusively active on mannan has been reported.

124   Here, we report a detailed functional characterization of *Ri*CE2 and *Ri*CEX - two acetyl

125   mannan esterases (AcMEs) from *R. intestinalis*. The esterases have complementary

126   substrate specificities and act in tandem to deacetylate glucomannan and

127   galacto(gluco)mannan. Furthermore, we report the first structure of an AcME with a

128   mannopentaose co-crystallized in the active site, revealing how the two-domain

129   architecture of *Ri*CEX facilitates specificity towards the axially oriented 2-*O*-acetylation. To

130   the best of our knowledge, this structure is also the first carbohydrate esterase of any kind

131   crystallized with a substrate in the active site.

132

133   **Results and discussion:**

134   A gene cluster in *R. intestinalis* encoding mannan degrading enzymes (20) contains

135   two acetyl esterases, *Ri*CEX and *Ri*CE2. *Ri*CE2 is a 349 amino acid CAZy family 2 esterase

136   which shares 29.46% identity with the xylan esterase CjCE2C (also known as

137   CE2C;CJA_2889 and Axe2B) of *Cellvibrio japonicus* (Uniprot accession no B3PC75) (24).

138   Analysis of the *Ri*CE2 sequence with InterProScan (28) identified the C-terminal residues

139   163-375 in *Ri*CE2 as an SGNH hydrolase domain, while residues 1-159 constitute a galactose

140   binding superfamily domain. This two-domain architecture is characteristic for CE2 family

141   esterases (23). BlastP searches (29) of *Ri*CEX (372 amino acids) returned very low sequence

142   homology to any characterized esterases (20% sequence similarity with acetyl xylan

143   esterase Axe2 of *Geobacillus stearothermophilus* (30). Despite the low similarity, the

144   sequence still appeared to be a promising esterase candidate, due to its location in the *R.*

145   *intestinalis* mannan PUL, and the N-terminal SGNH hydrolytic domain. Contrary to the CE2

146   family esterases, where the SGNH domains are present in the C-terminal, the *Ri*CEX

147   hydrolytic domain is present in the N-terminal residues 35-209. InterProScan (28) was not

148   able to predict a function for the 163 amino acid C-terminal domain of *Ri*CEX. This previously

149   uncharacterized sequence organization captured our interest for further structural

150   exploration.

151   Crystal structures for the *Ri*CEX with acetate (PDB ID code 6HFZ, 1.75 Å resolution)

152   and mannopentaose (PDB ID code 6HH9, 2.4 Å resolution) in the enzyme active site reveal

153   several structural feauteres. For the structure with mannopentaose, four mannose units

154   were observed in the electron density maps. The enzyme consists of two domains

155   connected by a linker of about 20 amino acids (Fig. 2A). The N-terminal domain (ca. 210

156   amino acids) displays an α/β-hydrolase (SGNH-hydrolase) fold while the C-terminal domain

157   (ca. 140 amino acids) comprises a jelly-roll beta-sandwich fold. Structural alignment of the

158   complete *Ri*CEX structure against the Protein Data Bank using PDBeFold (31) returned hits

159   with low scores, indicating this is a hitherto unidentified fold. The two structures with the

160   highest scores were Ape1, a peptidoglycan *O*-acetylesterase from *Neisseria meningitidis*

161   (Fig. 2B) (PDB ID code 4K40, Q-score 0.17) (32), and the *Cj*CE2B (Uniprot accession no.

162   F7VJJ8) carbohydrate esterase from *C. japonicus* (Fig. 2C) (PDB ID code 2W9X, Q-score 0.12)

163   (24). It is apparent that the second domain of these three enzymes adopts different

164   positions in space when aligning their catalytic SGNH domains (Fig. 2A-C). These differences

165   are not due to domain flexibility. For the Ape1 enzyme, the second domain is inserted in the

166   middle of the SGNH domain sequence and is kept in place by two short linkers consisting of

167   3-4 amino acids. The second domain in the *Cj*CE2B enzyme, located at the N-terminal end of

168   the SGNH domain, also adopts a very different position than that found for the C-terminal

169   domain in *Ri*CEX, connected to the SGNH domain via an eight-residue linker.

170   Structural alignment searches using the C-terminal, non-catalytic domain of *Ri*CEX,

171   identified a carbohydrate binding module 35 (CBM35), similar to that of *Clostridium*

172   *thermocellum* (Fig. 2D) (PDBid 2W1W, Q-score 0.39)(33). CBM35 modules have previously

173   been demonstrated to bind decorated mannans (34). The *Ri*CEX$_{CBM35}$ domain appears to be

174   involved in substrate recognition and binding, forming a lid over the SGNH-domain active

175   site (Fig. 2). Several hydrophobic amino acids, Ile79, Phe86, Ala89, Ile263, Leu330, Leu332

176   and Ile367, contribute to stabilize the inter-domain interaction together with the three pairs

177   of charged or polar amino acid residues Glu119-His338, His116-Glu337 and Gln85-Thr334

178   (Fig. 2).

179   In the active site of the SGNH domain, three residues Ser41, His193 and Asp190 form

180   the hydrogen-bonded catalytic triad, and the amide nitrogen atoms of Ser41 and Gly81 and

181   the $N^{\delta 2}$ of Asn110 line the oxyanion hole (Fig. 2E). The high 2-*O*-acetylation specificity of

182   *Ri*CEX can be explained by the ligand bound structure. Amino acids from both the SGNH and

183   CBM35 domains form specific interactions with the mannopentaose and aligns it such that

184   the C2-OH group is only 2.3 Å from the Ser41-OH group (O-O distance), close to the

185   oxyanion hole, which forms a cavity that fits an acetyl group. In the apo- *Ri*CEX structure we

186   can clearly see an acetate molecule in the oxyanion hole (Fig. 2E) and this arrangement

187   could represent a product complex. Such binding of acetate in absence of carbohydrate

188   substrate has also been observed for Ape1 (32). The binding of acetate indicates how

189   intermediates in the reaction may be positioned and provides structural insight useful for

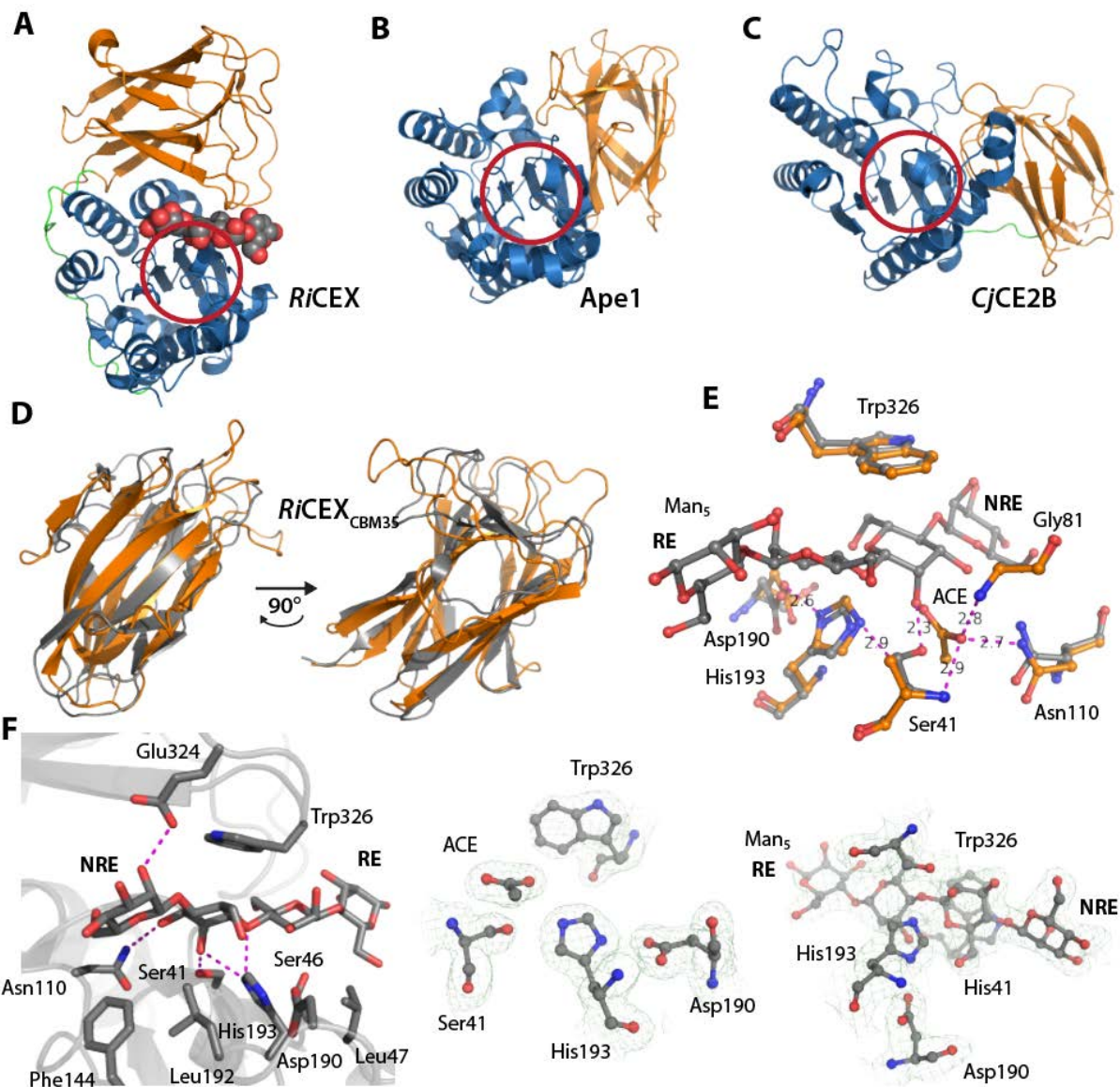190   further mechanistic studies.

191

192

193   Fig.2. Comparison with *Ri*CEX homologues and structural details of *Ri*CEX. (A) Crystal structure of *Ri*CEX, with four of the

194   mannose residues present in mannopentaose (spheres) visible in the electron density map. The catalytic domain (blue) is

195   connected to the CBM35 domain (orange) by a linker region (green). Panels (B) and (C) display the structural homologs

196   Ape1 and *Cj*CE2B that are closest to *Ri*CEX in the PDB database, respectively. The catalytic domains (blue) in (B) and (C) are

197   oriented to superimpose with the *Ri*CEX catalytic domain in A). The red rings in panels (A-C) indicate where the residues of

198   the catalytic triad are located. In panel (D) the *Ri*CEX$_{CBM35}$ domain (orange) is superimposed on the *Ct*CBM35 domain

199   (grey) and shown at two rotations, demonstrating the highly similar folds. (E) Display of the *Ri*CEX superposed with acetate

200   (orange carbons, ACE denotes acetate) or mannopentaose (grey carbons) in the active sites. In both structures Asp190

201   form a hydrogen bond with His193 (2.6 Å). In the acetate bound structure the His193-N$^{\varepsilon 2}$ is hydrogen bonded with the

202   Ser41-OH O-atom (2.9 Å). The O-atom of the acetate molecule pointing towards the oxyanion hole is hydrogen bonded by

203   Ser41-N (2.9 Å), Asn110-N$^{\delta 2}$ (2.7 Å) and Gly81-N (2.8 Å), indicated by dotted magenta lines to the acetate molecule. In the

204   mannopentaose bound structure, the hydrogen bond between His193- $N^{\epsilon 2}$ and the Ser41-OH O-atom is replaced with a

205   Ser41-OH O-atom hydrogen bond to the C2-OH group of the mannose residue in the esterase catalytic site (2.3 Å), implying

206   that the Ser41 side chain change conformation during catalysis. (F) Several charged or polar residues form hydrogen bonds

207   to the mannopentaose ligand (Ser41, Asn110, His193 and Glu324). Ser46 may interact with the ligand through a water

208   bridge. The hydrophobic residues Leu47, Phe144, Leu192 and Trp326 are part of the ligand-protein contact surface. Trp326

209   plays an important role, stacking on top of the mannose residue in the active site. The electron density maps of the active

210   sites are shown to the right in panel (F). The non-reducing end (denoted NRE) and the reducing end (denoted RE) are

211   labelled in the mannooligosaccharide ligand to aid interpretation of the figures.

212

213   Fig. 2F shows interactions between RiCEX and the mannopentaose ligand. Two

214   amino acids from the RiCEX$_{CBM35}$ domain contribute to ligand binding, namely Glu324 and

215   Trp326. The Glu324 forms a hydrogen bond to the O2 hydroxyl group of the mannose at the

216   non-reducing end next to the active site (subsite -1 according to Hekmat et al (35)).

217   Aromatic amino acids are often involved in protein-carbohydrate interactions, and in RiCEX

218   the Trp326 amino acid side chain stacks on top of the mannose unit in the active site. The

219   CBM35 appears to play a central role in reactivity of the enzyme. A truncated version of the

220   enzyme, containing only the catalytic domain, was not active either on natural substrates, or

221   pNP (p-Nitrophenol or 4-Nitrophenol) acetate Fig. S1). An observed lack of activity of the

222   SGNH domain indicates that it does not have an inherent esterase activity alone, but rather

223   has adapted to 2-O-deacetylation by interaction with the CBM35 domain. The activity

224   appears to depend on the two domains forming a confining clamp that provides substrate

225   interactions and aid protein stability. This hypothesis was further supported by the results of

226   thermal shift assay (Fig. S2), which showed a decrease in stability for the SGNH domain (as

227   compared with the complete RiCEX), and a lack of folding for the CBM35 domain.

228   Interestingly, the two-domain arrangement results in cavities or clefts on each side of the

229   active site indicated by the two green and magenta patches in Fig. 3A. Both these cavities

230   are arranged so that galactose residues linked to the mannose backbone (corresponding to -

231   1 and +1 subsites) at the O-6 position would point towards these spaces. This feature may

232   be important for recognizing galactose decorated mannans and may also influence the

233   substrate specificity of the enzyme.

234   Since mannan degradation is a common process in many microbial ecosystems, we

235   searched for microbes carrying protein sequences related to RiCEX. Searching the UniProtKB

236   database with a Hidden Markov Model (HMM, detailed description in the supplementary

237   information) of both domains of RiCEX, we identified 449 protein sequences with the same

238   two-domain architecture. Sequence alignment using MView showed that the catalytic triad

239   (Ser41, His193 and Asp190) and the Trp326 of the CBM domain were conserved in the 90%

240   consensus sequence (Fig. S3). While a vast majority of *Ri*CEX homologues came from the

241   phylum *Firmicutes* (435), 16 hits were identified in *Bacteroidetes.* Analysis of the

242   neighbouring genes in both Firmicutes and Bacteroidetes genomes and alignment of *Ri*CEX

243   along with five of its homologues (Fig. S4) from taxonomically distant bacterial taxa suggests

244   that the active site arrangement might be adapted to a wider range of roles than just

245   deacetylation of β-mannans.

246   To assess if the conserved residues correspond to functionally important structural

247   features of *Ri*CEX, a subset of 77 sequences was selected from the HMM results by using a

248   more stringent E--value, and the conservation pattern was projected on the *Ri*CEX protein

249   surface using the ConSurf Server (Fig. 3B) (36)**.** Highly conserved amino acid residues

250   (magenta), semi-conserved (white) and variable residues (blue) are indicated, and it is

251   apparent that both the SGNH and CBM35 domains contribute with conserved residues

252   around the substrate binding site. The residues Ser41, Asn110, His193, Leu47, Phe144,

253   Leu192 of the of SGNH domain and Trp326 of the CBM35 domain are all conserved and are

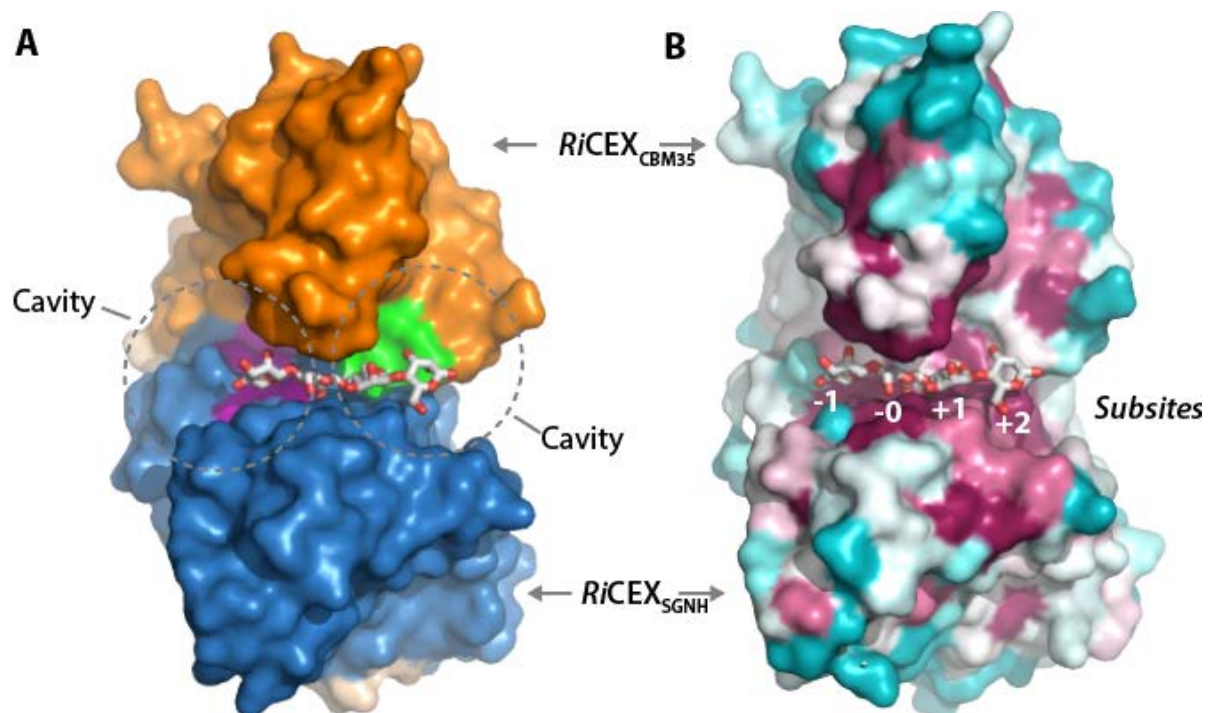254   interacting with the substrate in the active site.

255

256

Fig. 3. The 3D structures of substrate and product complexes of *Ri*CEX. (A) the magenta and green patches in the interface between the *Ri*CEX catalytic domain and the *Ri*CBM35 domain indicate cavities on the enzyme surface that may bind galactose residues decorating galactoglucomannan at the C6 position. In panel (B) the conservation score derived by ConSurf is projected on the *Ri*CEX surface. The magenta patches indicate highly conserved residues, which are concentrated around the substrate binding site. Subsites are labelled below the substrate according to the nomenclature suggested by *Hekmat et al (35).*

263

The mannan PUL in *R. intestinalis* encodes an extracellular mannanase - *Ri*GH26 which breaks down mannan into oligosaccharides, which are then internalized via an ABC transporter deacetylated by the esterases and further metabolized (20). To approximate these conditions, mannans used in activity testing were hydrolyzed with *Ri*GH26 prior to deacetylation. The two esterases were active on a wide range of mannans but not on structurally similar substrates such as acetylated xylan, cellulose monoacetate or chitin oligosaccharides (Fig. S5). A selection of mannose-based substrates was used to examine the impact of galactosylations (Norway spruce mannan), mannose units with multiple acetylations (*Aloe vera* mannan) and different acetylation distributions (konjac mannan, and its chemically acetylated version) on enzyme activity. Neither *Ri*CE2 nor *Ri*CEX were active on birch xylan (as well as its hydrolysate produced with a GH10 xylanase from *R. intestinalis* (21)), cellulose monoacetate or chitopentaose (Fig. S5D and E). The deacetylation specificity was the same on all mannans: there was a partial deacetylation seen whenever one of the esterases was used on its own (red and blue traces Fig. 4A and S5A-C and F). When the two

278   esterases were used together, a complete deacetylation was observed (purple traces Fig. 4A

279   and S5A-C and F).

280   Commercially available and in-house produced substrates contain a wide range of

281   acetylations present in a variety of positions on a mannose unit, and different locations in

282   the oligosaccharide chain, making it challenging to precisely determine the specificity of

283   esterases. In transesterification reactions, non-acetylated substrates are treated with

284   esterases in the presence of an appropriate acyl donor, resulting in an amount of highly

285   specific acetylated oligosaccharides consistent with the free energy of the reaction.

286   Transesterification with vinyl acetate has been used as a measure of substrate specificity of

287   acetyl esterases before (37). To further explore the substrate specificity of *Roseburia*

288   esterases, we used vinyl-acetate, -propionate and -butyrate as acyl donors. Both enzymes

289   were able to transacetylate and transpropylate (although to a much lesser extent than

290   acetylate) but not transbutyrylate mannotriose (Fig. 4 and S6). Both esterases were able to

291   transacetylate all mannose-based substrates tested, including mannooligosaccharides with

292   DP range 2-6, 6^1-α-D-galactosyl-mannotriose, 6^3, 6^4-α-D-galactosyl-mannopentaose, as well

293   as hydrolysates of AV mannan and Norway spruce GGM produced in house (Data not

294   shown).

295   As a means of demonstrating specificity transacetylation experiments were

296   performed on a mixture of mannotriose, cellotetraose and xylopentaose, with vinyl-acetate,

297   -propionate and -butyrate as ester donors. Acetylated mannotriose was the only product

298   observed in the MALDI ToF spectra (Fig. 4B), clearly indicating the mannan acetylesterase

299   specificity of *Ri*CEX and *Ri*CE2.

300
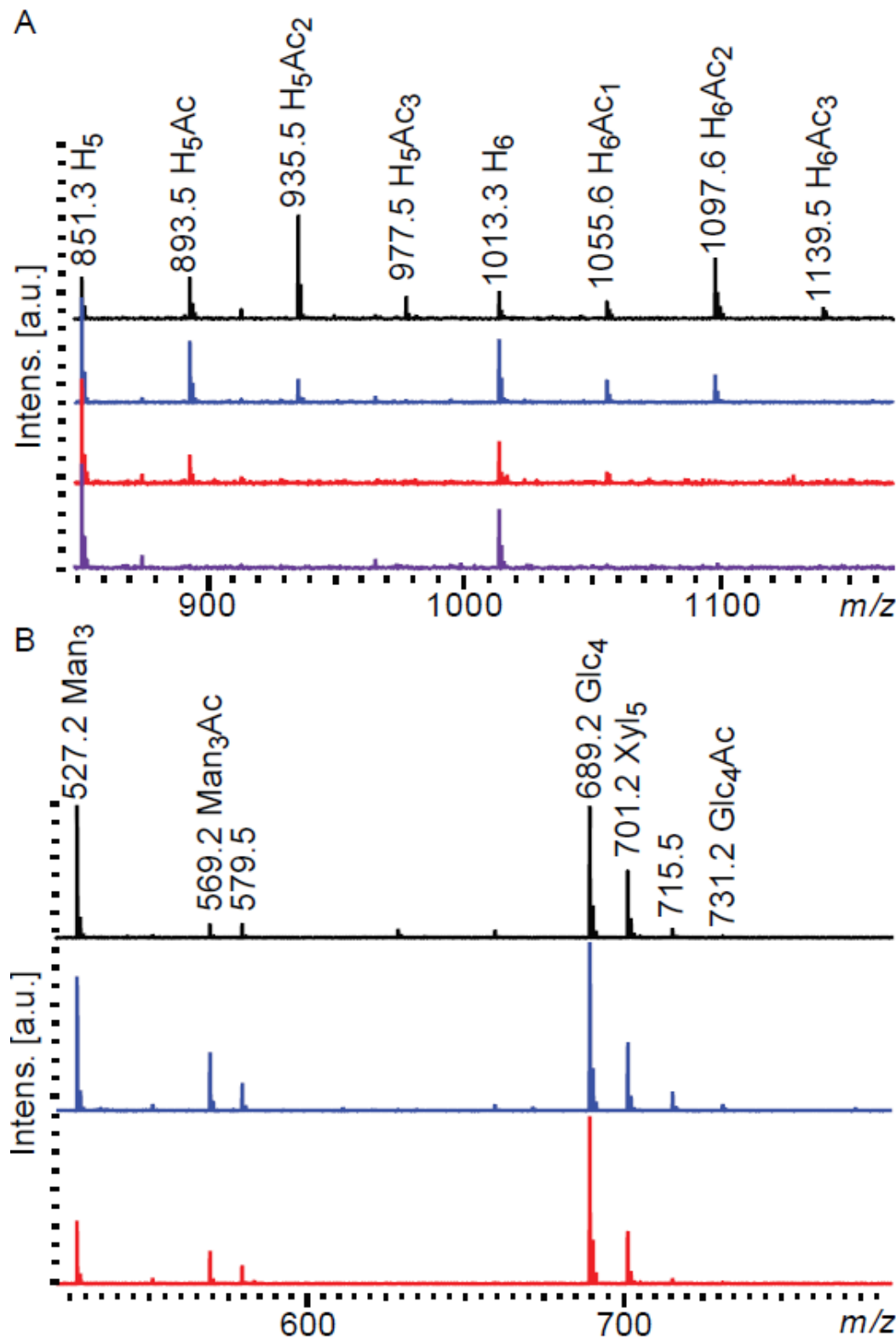
Fig. 4. MALDI-ToF spectra of deacetylation and transesterification reactions. (A) 10 mg/mL Spruce GGM hydrolysate (untreated in black) was treated with *Ri*CE2 (in blue), *Ri*CEX (in red) and the two enzymes in combination (purple). When either of the esterases was used, a decrease in the intensites of peaks signifying acetylated oligosaccharides was observed. Using the two enzymes in combination lead to a complete deacetylation of spruce mannan. (B) Transesterification of a mixture of 1 mg/mL of mannotriose, cellotetrose and xylopentose with a mixture of vinyl acetate, propionate and butyrate. No spontaneous esterification was observed (black trace). Out of all possible substrate combinations, both *Ri*CE2 (in blue) and *Ri*CEX (in red) produced acetylated mannotriose as the primary product. *Ri*CE2

309   produced a minor amount of acetylated cellotetraose (*m/z* 731) as a by-product. H- hexose, Glc- glucose, Man- mannose,
310   Xyl- xylose, Ac – acetylation.

311   The partial deacetylation observed in Fig. 4 and S5 warranted more detailed analysis

312   of the deacetylation preferences of the esterases. NMR analysis (Fig. 5) revealed that the

313   partial deacetylation seen in *Ri*CEX-treated samples was due to the fact that *Ri*CEX

314   exclusively removed all 2-*O*-acetylations from AV and Norway spruce GGM (Fig. 5B and 5F,

315   respectively). *Ri*CE2 removed the 3-*O*- and 4-*O*- acetylations as well as some of the 6-*O*-

316   acetylations from single acetylated mannose units in the same substrates (Fig. 5C and 5G).

317   Importantly, in the AV samples which contained a high number of double acetylated

318   mannose, *Ri*CE2 was not able to remove the 3-*O*- and 6-*O*- acetylations present on the same

319   mannose as a 2-*O*-acetylation (Fig. 5C). Adding *Ri*CEX to the solution of AV after the *Ri*CE2

320   enzymatic treatment and vice versa lead to a complete deacetylation of both substrates

321   (Fig. 5D and 5H), indicating that the two esterases have interdependent specificities, and are

322   both required for complete deacetylation of mannans.

323   *Ri*CE2 is a broad specificity esterase capable of removing 3-*O*-, 4-*O*- and 6-*O*-

324   acetylations, although its activity is limited by the presence of 2-*O*-acetylations as one of

325   multiple acetylations on a single mannose. This dependence of *Ri*CE2 on *Ri*CEX was also

326   observed in the reaction rates calculated from time-resolved NMR analysis of reactions with

327   AV as the substrate. Reaction rates showed that *Ri*CE2 was much slower when 2-*O*-

328   acetylations were present (Table 1). The presence of 3-*O*- and 6-*O*- acetylations on the same

329   mannose residues containing 2-*O*-acetylation did not affect the apparent k_{cat} of *Ri*CEX, while

330   the turnover rate of *Ri*CE2 more than doubled when 2-*O*-acetylations were removed (Table

331   1). *In vivo*, the enzyme pair would act in complement, with the specialist *Ri*CEX removing the

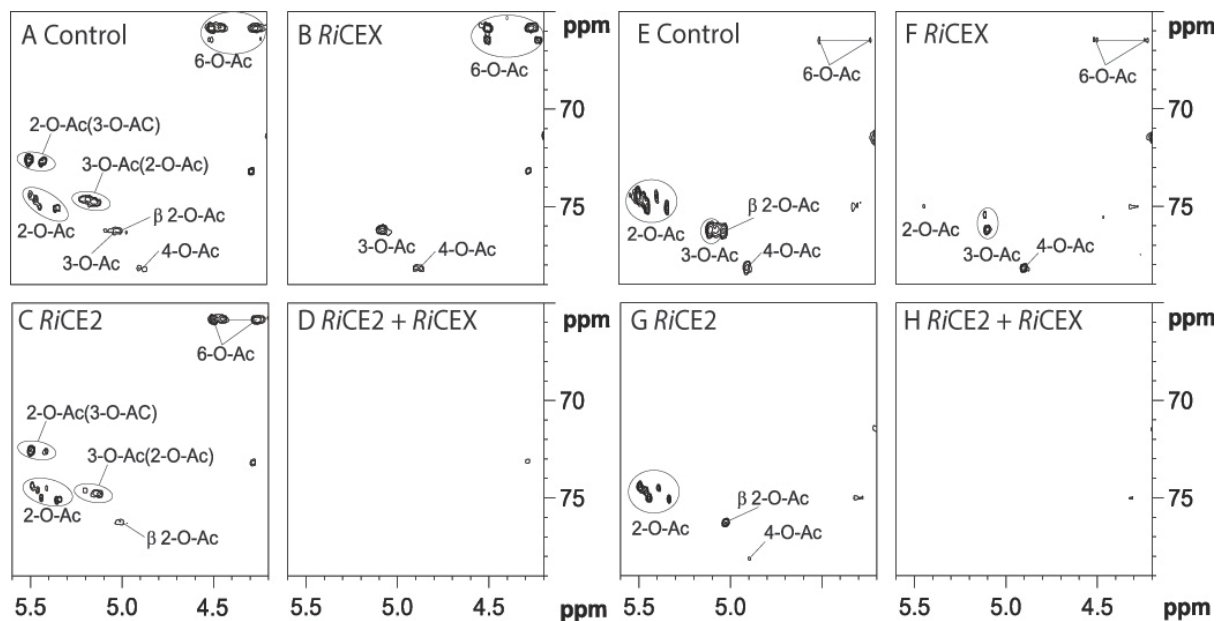332   2-*O*-acetylations that limit the activity of the generalist *Ri*CE2.

333

Fig. 5. 2D ^{13}C HSQC NMR spectra for area of interest of AV mannan RiGH26 hydrolysate (panels A-D) and Norway spruce mannan RiGH26 hydrolysate (panels E-H) treated with the esterases. (A) AV hydrolysate without enzyme addition, contained a high degree of acetylation on all possible positions, and a high degree of double acetylation. (B) When treated with RiCEX, the peaks corresponding to 2-O-acetylations disappear, and the shift values for peaks corresponding to 3-O- and 6-O-acetylations change due to the removal of 2-O-acetylations from double acetylated mannoses. (C) Treatment with RiCE2 removed all the non-reducing end 4-O-acetylations, the majority of 3-O- acetylations, and some of the 6-O-acetylations. (D) Treatment with both esterases at the same time removed all acetylations. (E) Spruce mannan hydrolysate without enzyme addition contained prevalently 2-O-, some 3-O- acetylations, and a lower degree of 4-O- and 6-O-acetylation. (F, G) Both enzymes exhibited similar activity on spruce mannan as on AV. (H). Acetylations in parenthesis signify the adjacent acetylations on double acetylated mannose (2-O-Ac(3-O-Ac) - -2-O- acetylation adjacent to a -3-O-acetylation).

Activity assays using para-Nitrophenyl (pNP) acetate, which is a commonly used substrate when screening for esterase activities showed that both esterases appear to be most active near neutral pH (Fig. 6). Notably, pNP acetate was a highly inadequate substrate for RiCEX with the apparent turnover rate nearly 2 orders of magnitude lower than on Norway spruce GGM (Table 1). This is not surprising, considering the topology of the RiCEX active site and the structural difference between the planar phenol ring of pNP and the axially oriented 2-O-acetylation on D-Man$p$; however, this result highlights the necessity for careful selection of substrates and methods when measuring esterase activity.

Both esterases showed near identical k$_{cat}$ and specific activities (Table 1) on RiGH26 hydrolyzed Norway spruce GGM substrate. In deacetylation rate measurements at pH 7.0 and 35 °C (approximating intracellular conditions of a gut commensal bacterium), at equal loadings (25nM final concentration) of each esterase the apparent total rate of deacetylation was lower than when 50nM of either esterase was used on its own. The lower resulting rate of deacetylation suggests that the esterases were competing for substrate, an

361   effect observed previously in lignocellulose degrading enzyme cocktails (38). Reaction rates

362   obtained in time-resolved NMR showed an increase in the *Ri*CE2 activity after removal of 2-

363   *O*- acetylations. This effect was not observed in the activity on Norway spruce GGM (Table

364   1), since the substrate used had much fewer double acetylated mannose units.

365
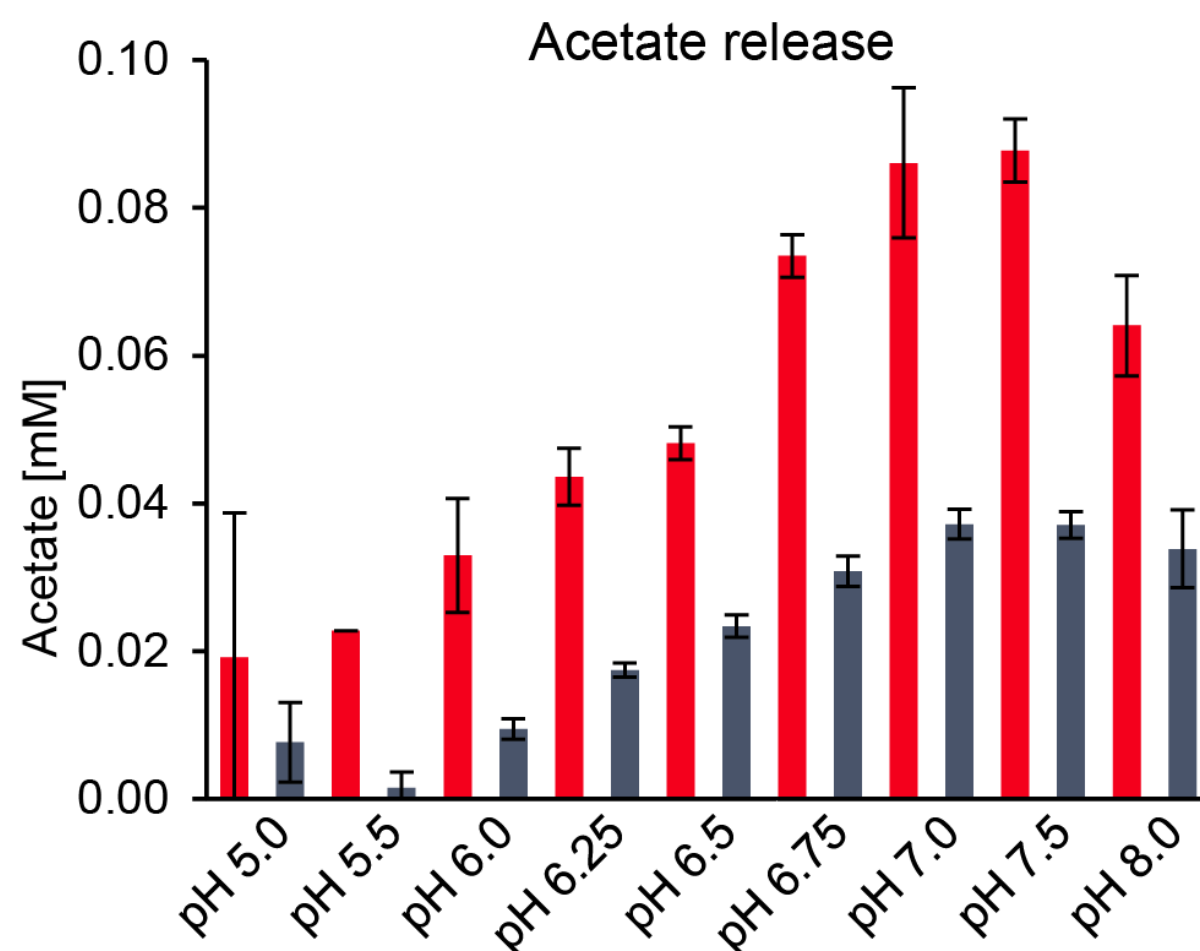
366
367   Fig. 6. pH optima of RiCEX (in red) and RiCE2 (in blue) as determined by the amounts of acetate released form pNP acetate
368   at different pH. Error bars indicate standard deviation between triplicates.

369

370

371

372   Table 1. Reaction rates of *Ri*CEX and *Ri*CE2. Turnover rate in time-resolved NMR analysis of deacetylation determined
373   based on the acetate released in the initial 15 minutes of reaction. Two identical samples of AV mannan hydrolysed with
374   RiGH26 mannanase were prepared and treated with 1) 62.5 nM loading of *Ri*CE2 for 16 hours, at 298.1 °K, then 10 nM
375   loading of *Ri*CEX 2) 10 nM loading of *Ri*CEX for 16 hours, then 62.5 nM loading of *Ri*CE2. Turnover rate and specific activity
376   [nanomole acetate/s/µg enzyme] of esterases on Norway spruce GGM RiGH26 hydrolysate were determined based on the
377   amounts of acetate released from samples of 100mg/mL of substrate in 30 minutes. Turnover rates of both esterases on
378   pNP acetate appear lower than on oligosaccharides.

Turnover rates and specific activities on oligosaccharides and pNP acetate.		
Time resolved NMR data on *Aloe vera* GGM:		

	*Ri*CEX	*Ri*CE2 after *Ri*CEX	
k_{cat} [s^{-1}]:	4.8	4.7	
	*Ri*CE2	*Ri*CEX after *Ri*CE2	
k_{cat} [s^{-1}]:	1.8	4.5	
Deacetylation of Norway spruce GGM:			
	*Ri*CEX	*Ri*CE2	*Ri*CE2 +CEX
k_{cat} [s^{-1}]:	73.5	76.7	41.7
specific activity:	1.7	1.9	-
Deacetylation of pNP acetate:			
	*Ri*CEX	*Ri*CE2	
k_{cat} [s^{-1}]:	0.93	40.00	

379 Footnote: Notably, the difference between catalytic activity on AV and Norway spruce cannot be directly compared due to
380 largely different reaction conditions (NMR experiments on AV were run at 298.1 °K/25 °C and pD 5.9 in a 5 mm NMR tube
381 whereas the Norway spruce GGM reactions 30 °C, pH 7.0 and 600 rpm shaking.

382

383   There is a growing body of evidence that acetylations on hemicellulose are prone to

384   migration on sugar rings and also across glycosidic linkages (39, 40). This phenomenon

385   requires particular attention when characterizing acetylesterases, since the distribution of

386   acetylations will change under certain conditions. Elevated pH and temperature (>90°C) are

387   known to induce acetyl migration on mannose and xylose (39, 41, 42). In experiments

388   conducted on monosaccharides, it has been shown that the acetyl groups migrate at pH >

389   6.0. In both D-glucose and D-galactose, acetylations initially present in the 2-*O*-position

390   appear to move in a 'clockwise' (2-*O*-→3-*O*-→4-*O*) direction at pD >7 (43, 44), while at pD

391   <3.0 D-galactose was shown to deacetylate without the acetyl group migrating (44). Notably,

392   we observed that migration happens also on the polymers and at even less severe

393   conditions. This phenomenon changes the properties of mannans as substrates and as

394   biorefining feedstocks. At pH 5.9 and 20°C *Ri*CEX transacetylated all three Man*p* units of

395   mannotriose, exclusively in the 2-*O*- position (Fig. S7 A) without any observed migration

396   occurring. Exposure to just 60°C for one hour at pD 5.9 (Fig. S7 B), incubation at pD 7.4 at

397   room temperature (Fig. S7 C), or incubation pD 7.4 at 60°C (Fig. S7 D), caused a decrease in

398   the signals for 2-*O* acetylations and an appearance of signals for 3-*O*-, 4-*O*- and 6-*O*-

399   acetylations, the latter two only in the non-reducing end mannose. At these conditions, the

400   acetylations on the non-reducing end migrated in the same 'clockwise' 2-*O*- → 6-*O*-

401   direction as described before on Gal*p* monosaccharides (41). The glycosidic bond prevents

402   migration from 3-*O*-→ 6-*O*- and thus limit the migration from 2-*O*-/3-O-→6-*O*- for the

403   reducing end and the intra-chain Man*p*. Migration pictured in Fig. S7 has progressed until an

404   apparent equilibrium of acetyl distribution was reached, with a proportion of the

405   acetylations remaining on the 2-*O*- position. Using the 2-*O*- deacetylation specificity of

406   *Ri*CEX, we were able to produce a sample of Norway spruce GGM with all 2-*O*- acetylations

407   removed. We examined the acetylation levels in solutions of Norway spruce GGM exposed

408   to migration invoking conditions, then treated with *Ri*CEX to remove newly accumulated 2-

409   *O*- acetylations. Both pH increase (Fig. S8) and heating to 60 °C for one hour (Fig. S9)

410   induced a re-distribution of acetylations resulting in new 2-*O*- acetylations. Treatment with

411   *Ri*CEX and repeated migration resulted in a complete removal of acetylations by only

412   removing the 2-*O*- bound acetyls. This indicates that the acetyl migration does not proceed

413   in a particular direction, but rather is a re-distribution process. A detailed description of

414   acetyl migration is provided in the supplementary information.

415

416   **Concluding remarks**

417   This study provides detailed insight into enzymatic deacetylation of β-mannans by

418   the abundant human gut commensal bacterium *R. intestinalis*. The deacetylation apparatus

419   of *R. intestinalis* consists of the highly specialized 2-*O*-acetylation specific *Ri*CEX, and *Ri*CE2

420   that removes all remaining types of acetylations. Both enzymes are necessary for

421   deacetylation, and their activities are complementary. Both esterases have a two-domain

422   structure with an SGNH superfamily hydrolytic domain and an accessory domain – a

423   galactose binding superfamily domain in *Ri*CE2 and a CBM35 in *Ri*CEX.

424   Selective activity of *Ri*CEX was instrumental in our study of acetyl migration on

425   mannooligosaccharides. We have demonstrated that acetyl migration proceeds towards the

426   2-*O*- position when the acetylations in that position are removed from an oligosaccharide.

427   Our results show explicitly that the choice of substrate and reaction conditions is crucial for

428   studying the specificity of hemicellulose esterases.

429   The potential for industrial application of this enzyme pair is quite apparent. With

430   the activity on gluco- and galacto(gluco)mannans, the pair could be applied to various

431   mannan-containing feedstocks to reduce the recalcitrance of mannans, modify the viscosity

432   of mannans in solution, or to rationally design oligosaccharides with distinct esterification

433   patterns via specific deacetylation or transesterification.

434

435   **Acknowledgments:**

436   Cellulose monoacetate with a degree of acetylation of 0.6 was a kind gift from Qi

437   Zhou (KTH, Stockholm). A chemically acetylated konjac glucomannan prepared according to

438   Bååth et al. (45) was kindly provided by Francisco Vilaplana. Norwegian Research council

439   grant no. 244259, 208674/F50, 226244, and 226247 supported this work.

440
441
442   **Materials and Methods:**

443

444   Enzymes.

445   Recombinant *Ri*CEX (ROSINTL182_05471) and *Ri*CE2 (ROSINTL182_05473) were produced in

446   *Escherichia coli* BL21 Star (DE3) as described previously (46). Truncated versions of *Ri*CEX

447   and seleno-L-methionine substituted *Ri*CEX were produced as described in SI Materials and

448   Methods.

449

450   Substrates.

451   Galactoglucomannan from Norway spruce (*Picea abies*) and glucuronoxylan from Birch

452   (*Betula pubescens*) were produced in house from dried wood chips. The wood was milled

453   into <2mm particles, and steam exploded at 200°C (10 minutes reactor residence time) in 5-

454   6 kg batches. The liquid soluble fraction containing the hemicelluloses was extracted by

455   washing the steam-exploded material with MilliQ water in a 50 µm pore WE50P2VWR bag

456   filter (Allied filter systems, England). The liquid fraction of hemicellulose was then filtered

457   through a 5 kDa spiral wound Polysulphone/polyethersulphone polyester ultrafiltration

458   membrane (GR99PE, Alfa Laval, Denmark) using a GEA pilot scale filtration system Model L

459   (GEA, Denmark). The fraction retained by the membrane was concentrated, collected and

460   freeze-dried to become the Norway spruce GGM sample. Birch xylan was produced

461   according to the protocol described in Biely *et al*. (47). 6^1-α-D-Galactosyl-mannotriose; 6^3,

462   6^4-α-D-Galactosyl-mannopentaose, penta-N-acetylchitopentaose, mannotriose,

463   mannotetrose, mannopentaose, konjac and carob mannans were purchased from

464   Megazyme, Ireland. *Aloe vera* mannan (Acemannan) was purchased from Elicityl, France.

465   Norway spruce GGM and *Aloe vera* mannan were hydrolysed with *Ri*GH26 in an unbuffered

466   solution. Samples were then filtered through a pre-washed 1 mL Amicon Ultracel 3kDa

467   ultrafiltration device (Merck KGaA, Germany) to remove the hydrolase and freeze dried.

468

469   Activity analysis.

470   Activities of the enzymes were tested by adding 1 µM of enzyme to 10 mg/mL solutions

471   of carbohydrate substrates listed above. All substrate solutions were prepared with 20 mM

472   sodium phosphate pH 5.9 to prevent acetyl migration. Reactions were incubated overnight

473   in 20 mM sodium phosphate pH 5.9 at 30°C with 700 rpm shaking. In some analyses, MilliQ

474   water was used instead of buffer to reduce background signals in MALDI-ToF MS as both

475   enzymes were found to be active without buffers.

476

477   Temperature and pH optima using 4-nitrophenyl acetate.

478   In order to determine the pH and temperature optima for the enzymes, reactions with

479   0.5 mM pNP acetate were prepared using 50 mM sodium phosphate buffer (Sigma-Aldrich,

480   Germany) in the pH range 5.5-8.0 (Sigma-Aldrich, Germany). pH optimum reactions were

481   incubated at 25 °C. Due to the difference in deacetylation rate of pNP acetate by the two

482   enzymes, 1 nM final concentration of RiCE2 and 0.1 µM of RiCEX were used in the pNP

483   acetate experiments. Standard plots of 4-Nitrophenol (p-Nitrophenol) were prepared at

484   each pH. To determine the optimum pH, 99 µL of sample mixture containing 1 mM of 4-

485   nitrophenyl acetate in each of the buffer were added to the wells of a 96 well plate. 1 µL of

486   enzyme solution was then added to the sample mixture and the reaction followed by

487   measuring the absorbance at 405 nm at one minute intervals. All experiments were

488   performed in triplicate, with two blanks for each condition set.

489

490   HPLC Measurement of acetate release.

491   Acetate content was analyzed on an RSLC Ultimate 3000 (Dionex, USA) HPLC using a

492   REZEX ROA-Organic Acid H+ 300x7.8mm ion exclusion column (Phenomenex, USA) at 65°C,

493   10 µL injection volume, with isocratic elution using 0.6 mL/min of 5mM H_2SO_4 as mobile

494   phase and a UV detector set to 210 nm.

495

496   Crystallography.

497   RiCEX and RiCE2 crystallization conditions were screened using several commercial high

498   throughput 96 condition sitting drop screens, using 20 mg/mL, 10 mg/mL and 5 mg/mL

499   solutions of protein in a 1:1 ratio with ready-mixed mother liquors (200 nL of each).

500   Screening plates were set up using a mosquito HTS liquid handling robot (ttp labtech, UK).

501   Crystals were observed in spot G8 of the INDEX HT screen (Hampton Research, USA),

502   containing 0.2M ammonium acetate, HEPES pH 7.5 and 25% w/v PEG 3350. Hanging drop

503   optimization grids were manually set up with 0.2 M ammonium acetate, HEPES pH 7.0, 7.5

504   and 8.0, 20%, 25% and 30% w/v PEG 3350. Crystallization liquor was mixed 2 μL:2 μL and 1

505   μL:1 μL in the hanging drops, with additional 2 μL or 1 μL of 5 mg/mL solution of

506   mannotriose, mannotetrose and mannopentose (Megazyme, Ireland) for co-crystallization.

507   Crystals were transferred to a cryo-solution containing mother-liquor with 35 % glucose

508   before flash freezing in liquid nitrogen. Diffraction data were collected at beamlines ID23-1

509   and ID-29 at the European synchrotron Research Facility in Grenoble, France. For additional

510   information on X-ray data collection, see supplementary material.

511   The initial structure was solved by single-wavelength anomalous diffraction (SAD) using

512   selenomethionine to obtain an anomalous signal. Data was processed by XDS (48) and

513   scaled by AIMLESS (49). The Phenix software package (50) was used to phase (AUTOSOL)

514   (51) and build (AUTOBUILD) (52) the first structure. Subsequent structures were solved by

515   molecular replacement (Phaser) (53) and refined using REFMAC (54). Model manipulations

516   were carried out using Coot (55) and molecular graphics were generated using Pymol2

517   (Schrödinger).

518

519   MALDI-ToF analysis:

520   MALDI-ToF analysis of hydrolysis products was conducted on an UltraFlextreme MALDI-

521   ToF instrument (Bruker Daltonics GmbH, Germany) equipped with a nitrogen 337 nm laser

522   beam. Samples were prepared by mixing 2 μL of a 9 mg/mL solution of 2,5-dihydroxybenzoic

523   acid (Sigma-Aldrich, Germany) in 30% acetonitrile (VWR) to an MTP 384 ground steel target

524   plate (Bruker Daltonics GmbH, Germany) and 1 μL of hydrolysate (0.1-1 mg/mL). Sample

525   drops were then dried under a stream of warm air.

526

527   Preparative HPLC, transesterification and NMR experiments are described in SI Materials

528   and Methods.

529

530   **References:**

531   1.   Strahl BD & Allis CD (2000) The language of covalent histone modifications. *Nature*
532   403(6765):41-45.

533   2.   Ragland SA & Criss AK (2017) From bacterial killing to immune modulation: Recent insights
534   into the functions of lysozyme. *PLOS Pathogens* 13(9):e1006512.
535   3.   Sonawane VC (2006) Enzymatic Modifications of Cephalosporins by Cephalosporin Acylase
536   and Other Enzymes. *Critical Reviews in Biotechnology* 26(2):95-120.
537   4.   Gille S & Pauly M (2012) O-Acetylation of Plant Cell Wall Polysaccharides. *Frontiers in Plant*
538   *Science* 3(12).
539   5.   Biely P (2012) Microbial carbohydrate esterases deacetylating plant polysaccharides.
540   *Biotechnol Adv.* 30.
541   6.   Willfor S*, et al.* (2003) Characterisation of water-soluble galactoglucomannans from Norway
542   spruce wood and thermomechanical pulp. *Carbohyd Polym* 52(2):175-187.
543   7.   Lundqvist J*, et al.* (2002) Isolation and characterization of galactoglucomannan from spruce
544   (Picea abies). *Carbohydrate Polymers* 48(1):29-39.
545   8.   Simões J, Nunes FM, Domingues P, Coimbra MA, & Domingues MR (2012) Mass
546   spectrometry characterization of an Aloe vera mannan presenting immunostimulatory
547   activity. *Carbohydrate Polymers* 90(1):229-236.
548   9.   Singh S, Singh G, & Arya SK (2018) Mannans: An overview of properties and application in
549   food products. *International Journal of Biological Macromolecules* 119:79-95.
550   10.   Cosgrove D & Jarvis m (2012) Comparative structure and biomechanics of plant primary and
551   secondary cell walls. *Frontiers in Plant Science* 3(204).
552   11.   Willfor S, Sundberg K, Tenkanen M, & Holmbom B (2008) Spruce-derived mannans - A
553   potential raw material for hydrocolloids and novel advanced natural materials. *Carbohydrate*
554   *Polymers* 72(2):197-210.
555   12.   Du XZ, Li J, Chen J, & Li B (2012) Effect of degree of deacetylation on physicochemical and
556   gelation properties of konjac glucomannan. *Food Research International* 46(1):270-278.
557   13.   Mudgil D, Barak S, & Khatkar BS (2014) Guar gum: processing, properties and food
558   applications-A Review. *Journal of Food Science and Technology-Mysore* 51(3):409-418.
559   14.   Tester RF & Al-Ghazzewi FH (2013) Mannans and health, with a special focus on
560   glucomannans. *Food Research International* 50(1):384-391.
561   15.   Martens EC, Chiang HC, & Gordon JI (2008) Mucosal glycan foraging enhances fitness and
562   transmission of a saccharolytic human gut bacterial symbiont. *Cell host & microbe* 4(5):447-
563   457.
564   16.   Reeves AR, Wang GR, & Salyers AA (1997) Characterization of four outer membrane proteins
565   that play a role in utilization of starch by Bacteroides thetaiotaomicron. *Journal of*
566   *bacteriology* 179(3):643-649.
567   17.   Cockburn DW & Koropatkin NM (2016) Polysaccharide Degradation by the Intestinal
568   Microbiota and Its Influence on Human Health and Disease. *Journal of Molecular Biology*
569   428(16):3230-3252.
570   18.   Flint HJ, Scott KP, Duncan SH, Louis P, & Forano E (2012) Microbial degradation of complex
571   carbohydrates in the gut. *Gut Microbes* 3(4):289-306.
572   19.   Lloyd-Price J*, et al.* (2017) Strains, functions and dynamics in the expanded Human
573   Microbiome Project. *Nature* 550(7674):61-66.
574   20.   La Rosa SL*, et al.* (2019) The human gut Firmicute Roseburia intestinalis is a primary
575   degrader of dietary β-mannans. *Nature Communications* 10(1):905.
576   21.   Leth ML*, et al.* (2018) Differential bacterial capture and transport preferences facilitate co-
577   growth on dietary xylan in the human gut. *Nature Microbiology* 3(5):570-580.
578   22.   Lombard V*, et al.* (2010) A hierarchical classification of polysaccharide lyases for
579   glycogenomics. *Biochem J* 432(3):437-444.
580   23.   Nakamura AM, Nascimento AS, & Polikarpov I (2017) Structural diversity of carbohydrate
581   esterases. *Biotechnology Research and Innovation* 1(1):35-51.
582   24.   Montanier C*, et al.* (2009) The active site of a carbohydrate esterase displays divergent
583   catalytic and noncatalytic binding functions. *PLoS Biol* 7(3):e71.

584   25.   Topakas E, *et al.* (2010) Carbohydrate esterases of family 2 are 6-O-deacetylases. *FEBS Lett*
585   584(3):543-548.
586   26.   Tenkanen M, Puls J, Ratto M, & Viikari L (1993) ENZYMATIC DEACETYLATION OF
587   GALACTOGLUCOMANNANS. *Applied Microbiology and Biotechnology* 39(2):159-165.
588   27.   Tenkanen M, Thornton J, & Viikari L (1995) AN ACETYLGLUCOMANNAN ESTERASE OF
589   ASPERGILLUS-ORYZAE - PURIFICATION, CHARACTERIZATION AND ROLE IN THE HYDROLYSIS
590   OF O-ACETYL-GALACTOGLUCOMANNAN. *Journal of Biotechnology* 42(3):197-206.
591   28.   Finn RD, *et al.* (2017) InterPro in 2017—beyond protein family and domain annotations.
592   *Nucleic Acids Res* 45(Database issue):D190-D199.
593   29.   Altschul SF, *et al.* (1997) Gapped BLAST and PSI-BLAST: a new generation of protein database
594   search programs. *Nucleic Acids Res* 25(17):3389-3402.
595   30.   Lansky S, *et al.* (2014) A unique octameric structure of Axe2, an intracellular acetyl-
596   xylooligosaccharide esterase from Geobacillus stearothermophilus. *Acta Crystallographica*
597   *Section D* 70(2):261-278.
598   31.   Krissinel E & Henrick K (2005) Multiple alignment of protein structures in three dimensions.
599   *Computational Life Sciences, Proceedings* 3695:67-78.
600   32.   Williams AH, *et al.* (2014) Visualization of a substrate-induced productive conformation of
601   the catalytic triad of the Neisseria meningitidis peptidoglycan O-acetylesterase reveals
602   mechanistic conservation in SGNH esterase family members. *Acta Crystallographica Section*
603   *D-Biological Crystallography* 70:2631-2639.
604   33.   Montanier C, *et al.* (2009) Evidence that family 35 carbohydrate binding modules display
605   conserved specificity but divergent function. *Proceedings of the National Academy of*
606   *Sciences* 106(9):3065-3070.
607   34.   Boraston AB, Bolam DN, Gilbert HJ, & Davies GJ (2004) Carbohydrate-binding modules: fine-
608   tuning polysaccharide recognition. *Biochem J* 382(Pt 3):769-781.
609   35.   Hekmat O, Tokuyasu K, & Withers SG (2003) Subsite structure of the endo-type chitin
610   deacetylase from a deuteromycete, Colletotrichum lindemuthianum: an investigation using
611   steady-state kinetic analysis and MS. *Biochem J* 374(Pt 2):369-380.
612   36.   Ashkenazy H, *et al.* (2016) ConSurf 2016: an improved methodology to estimate and
613   visualize evolutionary conservation in macromolecules. *Nucleic Acids Res* 44(W1):W344-
614   W350.
615   37.   Kremnicky L, Mastihuba V, & Cote GL (2004) Trichoderma reesei acetyl esterase catalyzes
616   transesterification in water. *Journal of Molecular Catalysis B-Enzymatic* 30(5-6):229-239.
617   38.   Andersen N, *et al.* (2008) Hydrolysis of cellulose using mono-component enzymes shows
618   synergy during hydrolysis of phosphoric acid swollen cellulose (PASC), but competition on
619   Avicel. *Enzyme and Microbial Technology* 42(4):362-370.
620   39.   Mastihubová M & Biely P (2004) Lipase-catalysed preparation of acetates of 4-nitrophenyl β-
621   d-xylopyranoside and their use in kinetic studies of acetyl migration. *Carbohydrate Research*
622   339(7):1353-1360.
623   40.   Lassfolk R, *et al.* (2019) Acetyl Group Migration across the Saccharide Units in
624   Oligomannoside Model Compound. *Journal of the American Chemical Society* 141(4):1646-
625   1654.
626   41.   Roslund MU, *et al.* (2008) Acyl Group Migration and Cleavage in Selectively Protected β-d-
627   Galactopyranosides as Studied by NMR Spectroscopy and Kinetic Calculations. *Journal of the*
628   *American Chemical Society* 130(27):8769-8772.
629   42.   Kabel MA, de Waard P, Schols HA, & Voragen AG (2003) Location of O-acetyl substituents in
630   xylo-oligosaccharides obtained from hydrothermally treated Eucalyptus wood. *Carbohydr*
631   *Res* 338(1):69-77.
632   43.   Brecker L, Mahut M, Schwarz A, & Nidetzky B (2009) In situ proton NMR study of acetyl and
633   formyl group migration in mono-O-acyl D-glucose. *Magn Reson Chem* 47(4):328-332.

634 44. Roslund MU*, et al.* (2008) Acyl group migration and cleavage in selectively protected beta-d-
635   galactopyranosides as studied by NMR spectroscopy and kinetic calculations. *J Am Chem Soc*
636   130(27):8769-8772.
637 45. Arnling Bååth J*, et al.* (2018) Mannanase hydrolysis of spruce galactoglucomannan focusing
638   on the influence of acetylation on enzymatic mannan degradation. *Biotechnology for*
639   *Biofuels* 11(1):114.
640 46. Mackenzie AK*, et al.* (2015) A Polysaccharide Utilization Locus from an Uncultured Bacteroidetes
642   Phylotype Suggests Ecological Adaptation and Substrate Versatility. 81(1):187-195.
643 47. Biely P*, et al.* (2013) Mode of action of acetylxylan esterases on acetyl glucuronoxylan and
644   acetylated oligosaccharides generated by a GH10 endoxylanase. *Biochimica et Biophysica*
645   *Acta (BBA) - General Subjects* 1830(11):5075-5086.
646 48. Kabsch W (2010) XDS. *Acta Crystallographica Section D* 66(2):125-132.
647 49. Evans PR & Murshudov GN (2013) How good are my data and what is the resolution? *Acta*
648   *Crystallographica Section D* 69(7):1204-1214.
649 50. Adams PD*, et al.* (2010) PHENIX: a comprehensive Python-based system for macromolecular
650   structure solution. *Acta Crystallographica Section D* 66(2):213-221.
651 51. Terwilliger TC*, et al.* (2009) Decision-making in structure solution using Bayesian estimates of
652   map quality: the PHENIX AutoSol wizard. *Acta Crystallographica Section D* 65(6):582-601.
653 52. Terwilliger TC*, et al.* (2008) Iterative model building, structure refinement and density
654   modification with the PHENIX AutoBuild wizard. *Acta Crystallographica Section D* 64(1):61-
655   69.
656 53. McCoy AJ*, et al.* (2007) Phaser crystallographic software. *Journal of Applied Crystallography*
657   40(4):658-674.
658 54. Vagin AA*, et al.* (2004) REFMAC5 dictionary: organization of prior chemical knowledge and
659   guidelines for its use. *Acta Crystallographica Section D* 60(12 Part 1):2184-2195.
660 55. Emsley P, Lohkamp B, Scott WG, & Cowtan K (2010) Features and development of Coot. *Acta*
661   *Crystallographica Section D* 66(4):486-501.